Propagation of Intense Subpicosecond Laser Pulses through Underdense Plasmas

C. A. Coverdale, C. B. Darrow, and C. D. Decker
Lawrence Livermore National Laboratory, P.O. Box 808, Livermore, California 94550

W. B. Mori, K-C. Tzeng, K. A. Marsh, C. E. Clayton, and C. Joshi
Departments of Physics and Electrical Engineering, University of California, Los Angeles, California 90024
(Received 22 December 1994)

The propagation of an intense, subpicosecond laser pulse through a substantial length ($L/\lambda \sim 10^3$) of an underdense plasma ($n/n_c \sim 1\%$) is studied through experiments and computer simulations. For $I = 8 \times 10^{17}$ W/cm^2 only 55% of the incident laser light was transmitted through the plasma within the focal cone angle. The decrease in transmission was accompanied by Raman forward scattering as evidenced by the generation of anti-Stokes sidebands and up to 2 MeV electrons. Simulations show that the majority of the reduction in transmission could be due to Raman forward and side scattering.

PACS numbers: 52.40.Nk, 52.35.Mw, 52.40.Db, 52.65.Rr

During the past few years there has been a great deal of theoretical and computational work on the propagation of short-pulse, high-intensity laser pulses through underdense plasmas [1–4]. By this we mean pulse lengths less than the diffraction length, the plasma length, and the ion plasma period; intensities approaching 10^{18} W/cm^2 for 1 μm light; and plasma densities on the order 1% of the critical density. At these high intensities and low densities, electron-ion collisions are less important in determining the fraction of the energy that can be absorbed by a plasma of a given length. These laser pulses, however, are susceptible to many collective instabilities which can cause beam breakup. One of these instabilities is stimulated Raman forward scattering (SRS-F) [5], which is the decay of an electromagnetic wave (ω_0, k_0) into a plasma wave (ω_p, k_p) and two forward propagating electromagnetic waves at frequency $\omega_0 - \omega_p$ (Stokes) and $\omega_0 + \omega_p$ (anti-Stokes) where $\omega_p^2 = 4\pi e^2 n_0/m_e$. In this Letter, we show through experiments and supporting particle-in-cell (PIC) simulations clear evidence for the onset of SRS-F when a short-pulse (600 fsec), high-intensity (8×10^{17} W/cm^2) 1 μm laser pulse interacts with an underdense, $n = 2 \times 10^{19}$ cm^{-3}, gas jet plasma approximately 1 mm long. An experimental correlation is found between the onset of SRS-F and a decline in the fraction of the laser energy transmitted in the original focal cone. PIC simulations that closely model the experiment in two dimensions indicate that most of this reduction in transmission can be accounted for by absorption and scattering losses from SRS at near forward angles. These results may be important for the recently proposed fast-ignitor fusion concept [6], the self-modulated laser-wake field accelerator [3], and optical-field ionized x-ray laser schemes [7].

For conditions found in long pulse experiments, SRS-F had proven to be difficult to observe because the spatial gain across the plasma was limited and the temporal growth time was greater than an ion plasma period [8]. Therefore, there have been few previous experimental observations of the scattered light from SRS-F [9,10]. In fact, only Turner *et al.* [9] detected both the Stokes and anti-Stokes signals (a $0.2n_c$ plasma). Another diagnostic for SRS-F is the detection of energetic electrons [11] generated by the plasma wave which results from SRS-F. Joshi *et al.* [11] directly detected 1.8 MeV electrons from a $0.2n_c$ plasma while Turner *et al.* correlated the occurrence of the anti-Stokes light with keV x rays. The simultaneous observation of the anti-Stokes sidebands and energetic electrons is the strongest evidence for the excitation of SRS-F.

For short-pulse lasers, SRS-F is an absolute instability [1,2,4] in the frame of the laser pulse. The spatial-temporal theory of SRS-F predicts an asymptotic gain given by [4] $(2\pi G)^{-1/2}\exp[G]$, where $G = [8(P/P_c)(L/L_R)(\omega_p\tau)(\omega_p/\omega_0)]^{1/2}$, P_c is the critical power necessary for relativistic self-focusing [12,13], and $L_R = \pi w_0^2/\lambda$ is the Rayleigh length. For linearly polarized light $P/P_c = a_0^2(w_0^2/32)(\omega_p^2/c^2)$, where a_0 is the normalized vector potential of the laser, $a_0 = eA_0/mc^2$, and w_0 is the spot size. Therefore, for short pulses ($\omega_p\tau \approx 150$) and tenuous plasmas $\omega_p/\omega_0 = (n/n_c)^{1/2} = 0.1$, the laser power P needs to be of order P_c to observe SRS-F within a Rayleigh length (i.e., $G > 10$). We emphasize that SRS-F will continuously increase as P/P_c is increased from less than unity to greater than unity. For our laser parameters, the requirement that P/P_c be near unity necessitates a plasma density near 10^{19} cm^{-3} for 1 μm light. If the plasma is formed by field-induced ionization of a static fill gas, ionization induced refraction (IIR) limits the maximum plasma density that can be obtained to about 2×10^{18} cm^{-3} [14]. Therefore, to limit refraction and achieve the required density, the laser is focused into a supersonic gas jet target. For short pulses, stimulated Raman backscatter (SRS-B) grows spatially from the front of the pulse with a gain $\exp[(a_0/2\sqrt{2})(\omega_0/\omega_p)^{1/2}(\omega_p\tau)]$ [7]. This gain is generally large, and the instability eventually becomes

0031-9007/95/74(23)/4659(4)$06.00

strongly coupled [15], but the reflectivity is typically low because it saturates very rapidly at a local position within the laser pulse, limiting the amount of laser energy which can be coherently backscattered.

In the present experiments, a glass laser producing 1.053 μm, 600 fsec pulses with energies up to 3.0 J was used. The beam (8.4 cm diam, square profile in the near field) was focused by an aspheric lens (69 cm focal length, $f/8.2$) resulting in an Airy pattern at the focus [16] with an estimated maximum intensity of 1×10^{18} W/cm^2 $\pm$ 15% ($a_0 \approx 0.9$). In arriving at this result, we have used a Gaussian fit to the principal Airy lobe to deduce effective Gaussian beam waist spot sizes [17], $w_x = 13.6$ μm, $w_y = 20.4$ μm, of the slightly elliptical focal spot. The intensity follows from $I = 2E_A/(\tau \pi w_x w_y)$ [17], where $E_A = 0.84E_{\text{total}}$ is the energy contained in the principal Airy lobe [16]. Placing a gas jet, backed with helium, at the focus results in a tunnel-ionized plasma with a density controlled by varying the backing pressure (200–1000 psi). Using a second identical gas jet, the plasma length was measured to be 0.8 $\pm$ 0.1 mm [18]. The focal depth of the focused beam (distance between half-intensity points on each side of best focus) was measured to be 1.2 mm. While ideal Gaussian beam theory is not valid for relating the spot size and focal depth of an Airy beam, the previous discussion of SRS gain is applicable if we substitute beam intensities obtained in this manner when calculating a_0 and ignore the difference between our measured focal depth and the Gaussian Rayleigh range (since in these experiments the plasma length, ~0.8 mm, is less than a focal depth). The frequency shift of the anti-Stokes light was used both as a measure of the plasma density and for monitoring the SRS-F.

Near forward scattered light (5°–7° from the laser axis) was collected and spectrally analyzed using a 0.25 m, 150 grooves/mm grating spectrograph coupled to a liquid nitrogen cooled CCD camera. Because the CCD sensitivity drops off rapidly beyond 1100 nm, the Stokes cascade at $\omega_0 - n\omega_p$ could not be measured. This also meant that we could not measure sidescatter redshifted by ω_p from the pump frequency though it is important in the overall energy balance, as discussed later. Within a narrow range of laser and gas jet operating parameters, the first and second anti-Stokes features were clearly observable. Figure 1(a) shows one such spectrum and the $\Delta\omega$ between the first and second anti-Stokes and between the pump and the first anti-Stokes is the same to within 3%.

Although not shown here, the density inferred from the frequency shift of the first anti-Stokes feature as a function of the backing pressure of the gas jet monotonically increased with pressure, as expected [19]. Below 200 psi, the anti-Stokes was not observed because the SRS-F spatiotemporal growth is too small at the lower densities. On the high pressure side, an exponential increase in the amount of light near the pump frequency was observed and the anti-Stokes signal fell below the noise level. This

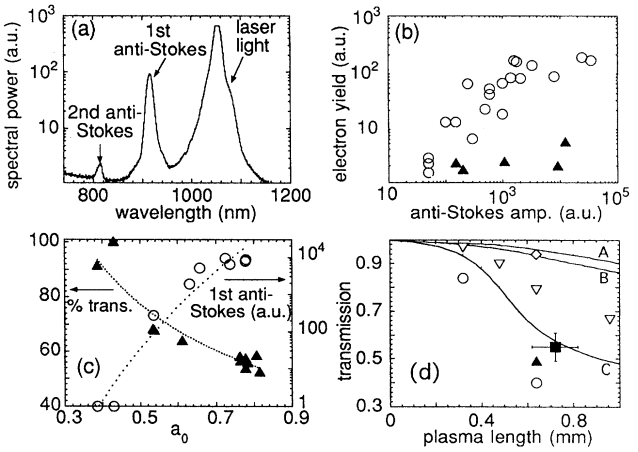

FIG. 1. (a) The frequency spectrum of the forward scattered light (5°–7° from the laser axis) and (b) the correlation of the 2 MeV electron signal with the amplitude of the first anti-Stokes (open circles). The solid triangles represent signal on the electron detector when the magnet polarity was reversed (null tests). (c) The variation of the transmitted laser energy (solid triangles) and the amplitude of the first anti-Stokes (open circles). (d) Transmitted power at all frequencies in the forward 2π steradians (lines) and at all frequencies in the cone angle of the beam (open symbols) vs propagation distance from PIC code simulations. The solid square represents the experimental transmission. The solid triangle is simulation result D.

could be due to a combination of diffraction caused by self-focusing from relativistic and plasma wave effects [20] and refraction caused by IIR [21]. Either effect could limit the net interaction length. The increase in scattered pump light occurred above 800 psi, whereas the anti-Stokes signal was maximum at this pressure (5 times larger than signals obtained at 600 psi and 1000 psi). The anti-Stokes signals were seen to disappear for both $P < 1.2P_c$, presumably because there is not a sufficient number of e foldings of growth, and $P > 5.3P_c$, where the laser pulse is intense enough for appreciable self-focusing and electron cavitation to occur [22]. At 800 psi, we determined the density of the plasma to be 2×10^{19} cm^{-3} from the frequency shift of the anti-Stokes signal.

To measure the high-energy electrons produced by SRS-F, a 90° bending magnet was placed 8 cm past the gas jet in the direct forward path of the laser. Electrons escaping the plasma in an $f/4$ cone were deflected by the magnet and detected using a 1 mm thick silicon surface-barrier detector (SBD). The magnetic field (1.5 kG) was chosen to collect 2.0 $\pm$ 0.1 MeV electrons. The SBD was shielded to minimize false electron signals from ambient x rays. Nevertheless, there is a background noise x-ray level on the SBD. Additional shielding blocked the line of site between the plasma region and the SBD, ensuring that electrons reaching the SBD were deflected with the magnet. On each laser shot we simultaneously measured the anti-Stokes signals, the 2 MeV electron signal, and, in addition,

the x-ray signal from a control detector. The control detector, an identical SBD, was placed about 15 cm from the gas jet 135° from the laser propagation direction. The electron and control detectors had identical lead shielding and a 50 μm copper foil in front to reduce the x-ray signal. The x-ray level on the electron SBD was measured by reversing the magnet polarity and correlating the x-ray signals measured on the two detectors. The electron-plus-x-ray signal was then measured on the electron detector with the correct polarity B field while the control detector measured the x-ray contribution. In this manner, the x-ray contribution (typically 10%) to the electron signal could be subtracted. The measured correlation of the electron signal and the first anti-Stokes level is shown in Fig. 1(b). These electron measurements were made at or near 800 psi, the pressure at which the anti-Stokes levels were highest. The electron signal was generally seen to increase with an increase in the anti-Stokes level (circles), whereas the x-ray noise level remained more or less constant.

In order to estimate the importance of SRS as a collective mechanism that can couple energy into plasma and also scatter light out of the cone angle of the incident beam, we measured the fraction of the incident laser energy transmitted through the original focal cone as a function of the incident laser energy for a backing pressure of 800 psi [Fig. 1(c)]. At low incident laser energy (<1 J), when no forward propagating collective instabilities were detected, the transmission was very nearly unity. We also measured the total amount of light backscattered in the cone angle of the beam. Even at the highest laser intensities used in this experiment, the total backscattered fraction was less than 2%, and therefore SRS-B and SBS (stimulated Brillouin scattering) [4] are negligible in the overall energy balance. As the incident laser energy was increased beyond 1 J ($P/P_c \approx 1.3$), the transmitted fraction began to decrease, as seen by the solid symbols in Fig. 1(c). At the highest energies (3.0 J, $P/P_c \approx 5.3$), only ~55% of the incident energy was transmitted in the cone angle of the laser beam. The decrease in the transmission was accompanied by a rapid increase (4 orders of magnitude) of the energy observed in the first anti-Stokes (open circles). This correlation of the decrease in the transmitted power and the increase in the level of the first anti-Stokes sideband strongly suggests that SRS at near forward angles is playing a role in reducing the transmitted fraction by depositing energy into the plasma and by scattering a substantial amount of laser light out of the cone angle being measured.

To quantify the role of the Raman forward and sidescatter in reducing the beam transmission, we have carried out two-dimensional PIC code simulations of the experiment. With the advent of massively parallel supercomputers it is now possible to model short-pulse, laser-plasma experiments far more realistically than in the past; i.e., the transverse and longitudinal spatial dimensions, laser pulsewidth, laser to plasma frequency ratio, and propagation distance in the simulation are the same as in the experiments. We have developed a parallelized fully relativistic electromagnetic PIC code which uses the basic algorithm of ISIS on a cyclic mesh [4,23]. The computational box is an 8192 × 256 Cartesian grid and the simulations follow 1.2×10^7 particles for 3×10^4 time steps. The main difficulties with quantitatively modeling the experiment are that the noise in the simulation is typically larger than in the experiment and that the simulations are two dimensional (slab geometry). In the recent experiment, however, SRS-B saturates so rapidly that it is rather insensitive to the noise source, and the SRS-F noise source is the ponderomotive wake which is independent of the thermal fluctuations [4].

In order to model the experimental conditions, an estimate of the effective plasma length is required. This estimate was made by performing a series of simulations which covered a range of laser intensities and plasma densities: (A) $\omega_0/\omega_p = 10$, $a_0 = 0.33$, and $P/P_c = 0.41$; (B) $\omega_0/\omega_p = 10$, $a_0 = 0.8$, and $P/P_c = 2.7$; and (C) $\omega_0/\omega_p = 5$, $a_0 = 0.5$, and $P/P_c = 4.0$. In each simulation, the laser spot size w_0 was 18 μm, the laser pulse duration was 600 fsec, the plasma was preformed with a uniform density, and the ions were immobile. The evolution of the electron distribution function, the electromagnetic mode spectra, and the laser energy transmitted through the original focal cone were monitored as a function of the distance the head of the laser pulse penetrated into the plasma. The results are summarized in Figs. 1(d) and 2(a)–2(d).

In Fig. 1(d) we plot the fraction of the total energy remaining in the electromagnetic modes at all frequencies (solid line) in the forward 2π steradians and the fraction remaining in the original focal cone of the beam (open symbols) as a function of the penetration distance for all three simulations. This plot clearly demonstrates

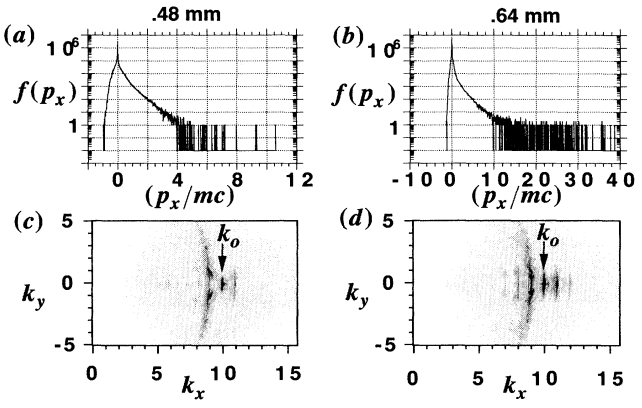

FIG. 2. From simulation B, the electron distribution function at (a) 0.48 mm and (b) 0.64 mm and the corresponding electromagnetic **k** spectrum at (c) 0.48 mm and (d) 0.64 mm (k_x and k_y are in units of ω_p/c).

that for a fixed penetration distance both the absorption and scattering losses increase with laser power and plasma density. These results are consistent with the experimental results in that, for low SRS-F gain ($G \leq 10$), very little transmission losses occur, while for high SRS-F gain ($G \geq 10$) significant transmission losses occur.

To make further quantitative comparisons, we examined the evolution of the electron distribution function and the first two anti-Stokes sidebands. In Fig. 2, we show for simulation B the electron distribution function $f(P_x)$ and the k spectrum of the laser, $E_z(k_x, k_y)$ after the pulse has penetrated 0.48 and 0.64 mm into the plasma. Figures 2(c) and 2(d) show that a substantial amount of light is sidescattered (SRS-S), as illustrated particularly by the Stokes line at $k_x = 9$. This sidescatter is extremely important in the overall energy balance. We calculate the total energy within each anti-Stokes line and find that after 0.64 mm (0.48 mm) the ratio of anti-Stokes/pump = 0.06 (0.006) and second anti-Stokes/anti-Stokes = 0.04 (in the noise). The experimentally measured ratios at 5°–7° for the anti-Stokes/pump and the second anti-Stokes/anti-Stokes were 0.034 and 0.027, respectively. The results from the experiment and the simulations are in reasonable agreement, within the shot-to-shot variation, for a plasma length of 0.64 mm. Importantly, this distance is less than the presumed dimension of the gas jet. In addition, the edge of the electron distribution does not exceed 2 MeV until the laser has penetrated 0.48 mm into the plasma [Fig. 2(a)], and it extends to 5 MeV after 0.64 mm of plasma, with a few electrons at 20 meV [Fig. 2(b)]. We emphasize that in simulation A ($P/P_c = 0.41$), no MeV electrons or higher order anti-Stokes sidebands were observed for laser penetration distances less than 1 mm.

Taking the plasma length to be 0.64 mm, we carried out an additional simulation (D) in which a laser pulse of $a_0 = 0.8$ was propagated through an $n = 2 \times 10^{19}$ cm^{-3} density plasma slab. These are the experimental conditions which gave the maximum transmission losses. In this simulation, only 49% of the laser light was transmitted through the $f/8$ focal cone, indicated in Fig. 1(d) as a solid triangle. This is in reasonable agreement with the experimental measurement of 55% [solid square in Fig. 1(d)]. The horizontal error bar on this symbol is indicative of the upper bound of uncertainty in the plasma length. We point out that the 51% loss in energy can be partitioned as 30% into Raman plasma waves and 20% into forward going sidescattered light. The degree to which the simulation and experimental results agree underscores the importance of SRS-F and SRS-S in preventing laser energy from propagating straight through an underdense plasma.

In summary, clear experimental evidence of stimulated Raman forward scatter from a short-pulse, high-intensity, laser-plasma interaction is presented. The onset of SRS-F is correlated experimentally with the emission of high-energy electrons and a decrease in the transmission of laser energy through the original focal cone. Two-dimensional PIC simulations confirm that this decrease in transmission is due mainly to a combination of Raman forward and sidescattering.

We would like to thank H. Nguyen, J. Crane, and M. D. Perry for their support of these experiments. This work was performed under the auspices of the U.S. Department of Energy by Lawrence Livermore National Laboratory under Contract No. W-7405-ENG-48 and at UCLA under DOE Grant No. DE-FG03-92ER40727 and LLNL Contracts No. B283617 and No. B283784.

[1] T. Antonsen and P. Mora, Phys. Rev. Lett. **69**, 2204 (1992).
[2] P. Sprangle *et al.*, Phys. Rev. Lett. **69**, 2200 (1992); E. Esarey *et al.*, Phys. Rev. Lett. **72**, 2887 (1994).
[3] J. Krall *et al.*, Phys. Rev. E **48**, 2157 (1993); N. E. Andreev *et al.*, JETP Lett. **55**, 577 (1992).
[4] W. B. Mori *et al.*, Phys. Rev. Lett. **72**, 1482 (1994); C. D. Decker *et al.*, Phys. Rev. E **50**, R3338 (1994).
[5] D. W. Forslund *et al.*, Phys. Fluids **18**, 1002 (1975), and references therein; K. Estabrook and W. L. Kruer, Phys. Fluids **26**, 1892 (1983).
[6] M. Tabak *et al.*, Phys. Plasmas **1**, 1626 (1994).
[7] P. Amendt *et al.*, Phys. Rev. Lett. **66**, 2589 (1991); N. H. Burnett and P. B. Corkum, J. Opt. Soc. Am. B **6**, 1195 (1989).
[8] D. W. Forslund *et al.*, Phys. Rev. Lett. **54**, 558 (1985).
[9] R. E. Turner *et al.*, Phys. Rev. Lett. **57**, 1725 (1986).
[10] S. H. Batha *et al.*, Phys. Rev. Lett. **66**, 2324 (1991); D. M. Villeneuve and H. A. Baldis, Phys. Fluids **31**, 1790 (1988); C. Labaune *et al.*, Phys. Fluids B **2**, 166 (1990).
[11] C. Joshi *et al.*, Phys. Rev. Lett. **47**, 1285 (1981).
[12] C. Max *et al.*, Phys. Rev. Lett. **33**, 209 (1974).
[13] P. Sprangle *et al.*, IEEE Trans. Plasma Sci. **PS-15**, 145 (1983); G. Schmidt and W. Horton, Comments Plasma Phys. Controlled Fusion **9**, 85 (1985).
[14] W. P. Leemans *et al.*, Phys. Rev. A **46**, 1091 (1992).
[15] C. B. Darrow *et al.*, Phys. Rev. Lett. **69**, 442 (1992).
[16] M. Born and E. Wolf, *Principles of Optics* (Pergamon Press, New York, 1964).
[17] A. E. Siegman, *Lasers* (University Science Books, Mill Valley, CA, 1986).
[18] C. Clayton and M. Everett (to be published).
[19] C. A. Coverdale, Ph.D. dissertation, University of California, Davis, 1995 (unpublished).
[20] P. Gibbon and A. T. Bell, Phys. Rev. Lett. **61**, 1899 (1988); W. B. Mori *et al.*, Phys. Rev. Lett. **60**, 1298 (1988).
[21] W. M. Wood *et al.*, Phys. Rev. Lett. **67**, 3523 (1991).
[22] G. Sun *et al.*, Phys. Fluids **30**, 526 (1987).
[23] C. D. Decker *et al.*, Phys. Rev. Lett. **72**, 490 (1994).

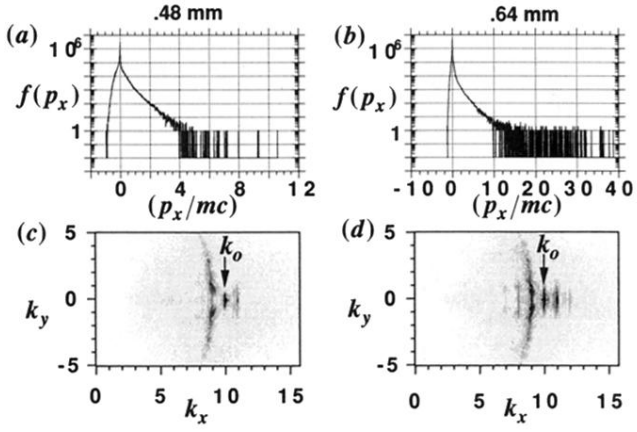

FIG. 2. From simulation B, the electron distribution function at (a) 0.48 mm and (b) 0.64 mm and the corresponding electromagnetic **k** spectrum at (c) 0.48 mm and (d) 0.64 mm (k_x and k_y are in units of ω_p/c).